CFSRC COLLOQUIUM

Proceedings of the Cold-Formed Steel Research Consortium Colloquium
20-22 October 2020 (cfsrc.org)

Extensions of the constrained Finite Strip Method for thin-walled members: closed sections and sections with rounded corners

Zhanjie Li[1], Sheng Jin[2]

Abstract

The objective of this paper is to provide a derivation for a constrained Finite Strip Method (cFSM) stability solutions that applied to thin-walled members with closed sections and sections with rounded corners. The current cFSM is able to provide the decomposed stability solutions for members with open sections – single branch and multi-branch. However, with the mode definitions and implementation adopted in current cFSM, there are limitations that inhabit its applications to other general sections, such as closed section, section with rounded corners, and curved sections. To overcome these limits, the traditional implementation approach of the Global (G), Distortional (D), and Local (L) modes through the warping displacement has been revisited and its relationship with the transverse displacements (i.e., Degree of Freedom, DOF) are then used to build the characteristics of these transverse displacements. Then, following the core assumptions of the mode definitions in current cFSM, a new implementation approach is adopted to establish the mode classes: through the transverse displacements instead of the warping displacement. Then, several other techniques are further introduced to enable the cFSM for overcoming the aforementioned limitations. First, the bredt shear strain for closed sections is incorporated along with the conventional in-place shear. Second, for section with rounded corners, the transverse DOFs, the controlling DOFs in the new implementation for the D modes are categorized into secondary DOFs (i.e., that can be determined from the controlling DOFs) whilst they are set as the controlling DOFs for L modes. Finally, numerical examples of several thin-walled steel members are illustrated to highlight the consistency of the new cFSM with current cFSM for open sections and the applicability to closed sections and sections with rounded corners.

1. Introduction

As a variant of the finite element method, the Finite Strip Method (FSM) developed by Y. K. Cheung [1] has been limitedly used in the structural analysis but still widely popular for the stability analysis of thin-walled members due to its unique longitudinal shape functions and the computational efficiency it can provide. In particular, this efficiency is demonstrated through the signature curve that can be obtained with the analytical FSM as populated by Hancock [2]. A series of solutions in terms of critical stresses as a function of buckling half-wavelengths can be obtained from the signature curve, through which the appropriate buckling modes of local, distortional, and global, commonly available in the thin-walled members, can be identified.

Meanwhile, the design specifications also explicitly require the determination of the strength of these three buckling modes separately. Some specifications such as AISI [3] also consider mode interactions among them (e.g., only L-G interaction is considered in AISI). Hence, several numerical methods were further developed in recent years to classify and categorize the buckling modes, such as Generalized Beam Theory (GBT) [4]–[7], constrained Finite Strip Method (cFSM) [8]–[11], and more recently constrained Finite Element Method (cFEM) [12]–[14]. Based on the mechanic definition of the buckling modes, all these methods can provide a definitive separation of the buckling modes. However, the classic cFSM implemented in CUFSM [15], [16] is limited to members with open-branch sections consisting of flat plate elements. To extend this to closed sections, Khezri and Rasmussen [17], [18] developed a new cFSM using an energy approach and Djafour et. al. using additional assumptions in cylindrical plate bending and negligible in-plane transverse strains and shear strains [19]. However, for curved sections such as circular cylindrical sections, even though the general FSM can approximate the sections with fined plate segments and obtain good buckling solutions, the cFSM is not able to extend to these approximated nodes for mode definitions. GBT implemented

[1] Associate Professor, Department of Engineering, SUNY Polytechnic Institute, zhanjie.li@sunypoly.edu
[2] Associate Professor, School of Civil Engineering, Chongqing University, civiljs@cqu.edu.cn

a new mode definition scheme for cylindrical sections [7]. In addition, the current cFSM is not able to handle the rounded corners given the node classification issues in mode definitions. Ádány [20] proposed a concept of elastic corner to approximate rounded corners for modal decomposition of thin-walled members. However, for large corner radii, the solution was found not quite satisfactory and this technique using elastic corner is not so direct from the mode definition point of view.

Meanwhile, new developments in GBT and cFSM, such as such as the energy approach by Becque [21] and Khezri and Rasmussen [17], [18], force-based approach by Jin et. al. [14], [22], and special assumptions by Djafour et. al. [19], explored the modified mechanical criteria for mode definitions to overcome some of the limitations of cFSM in closed sections and rounded corners. Some of these demonstrated the handlings of these limitations could potential be achieved through a different implementation approach even with the current mechanical criteria. Hence, in this paper, the enrichment of the current cFSM to overcome those limitation is explored. While using the same mechanical criteria such as Vlasov's hypothesis, etc., the implementation of these mode definition criteria will be modified. More specifically, , the traditional implementation approach of the Global (G), Distortional (D), and Local (L) modes through the warping displacement has been revisited and its relationship with the transverse displacements (i.e., Degree of Freedom, DOF) are then used to build the characteristics of these transverse displacements. Then, a new implementation approach is adopted to establish the mode classes: through the transverse displacements instead of the warping displacement. Several other techniques are further introduced to enable the cFSM for overcoming the aforementioned limitations: (1) the bredt shear strain for closed sections is incorporated along with the conventional in-place shear; (2) for section with rounded corners, the transverse DOFs, the controlling DOFs in the new implementation for the D modes are categorized into secondary DOFs (i.e., that can be determined from the controlling DOFs) whilst they are set as the controlling DOFs for L modes.

2. Mode definitions of thin-walled members based on the transverse deformation

The mode definitions of the traditional cFSM all starts with the warping characteristics of the G, D, and L based on the mechanical criteria, such as the Vlasov's hypothesis, derived from GBT. Based on the warping distribution, the transfer deformation of the cross section can be uniquely determined from the warping for the mode class, G, D, or L. This study explores an opposite route by defining the mode classes through transvers deformation instead of the warping.

2.1 Obtain the GDL's warping from their transverse deformation

Fig. 1 illustrates an open thin-walled cross section. As shown, there are n_M main nodes and n_M-1 plate elements. The sub-nodes are not illustrated here but will be introduced when needed.

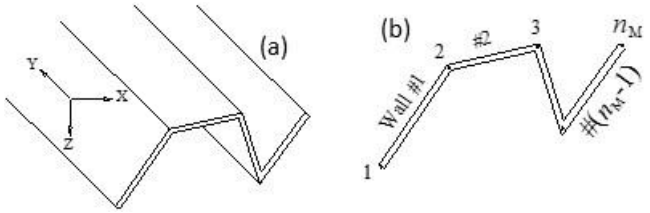

Fig. 1 (a) A thin-walled member and (b) the main nodes and plate elements

Based on the Valsov's hypothesis along with the longitudinal shape functions used in FSM [15], [23], the transverse displacement u of the middle-line of any plate i should satisfy:

$$u_i = \frac{a}{b_i \pi}(v_{\mathrm{M}j} - v_{\mathrm{M}k}) \tag{1}$$

where v_{Mj} and v_{Mk} are the longitudinal displacements (warping) at the two main nodes (i.e., *j* and *k*) of the plate element *i*. In current cFSM, apply Eq. (1) to all the plate elements results in:

$$\boldsymbol{u} = \boldsymbol{S}_1 \cdot \boldsymbol{v}_{\mathrm{M}} \tag{2}$$

This two equations illustrate the transverse displacements can be determined from the longitudinal displacements if the mode meets the Valsov's hypothesis. This process is not reversible given the fact that the open section has 1 more main nodes than the plate element number. However, if this the axial mode, which is orthogonal with all other GDL modes, was taken out from the G mode. This orthogonality can be written:

$$\int_A 1 \cdot v_{\mathrm{M}} \cdot \mathrm{d}A = 0 \tag{3}$$

In matrix form:

$$\mathbf{1}_{1\times n_{\mathrm{M}}} \cdot \boldsymbol{S}_2 \cdot \boldsymbol{v}_{\mathrm{M}} = 0 \tag{4}$$

Combine Eqs. (2) and (4), the invertible relation can be written:

$$\begin{Bmatrix} \boldsymbol{u} \\ 0 \end{Bmatrix} = \begin{bmatrix} \boldsymbol{S}_1 \\ \mathbf{1}_{1\times n_{\mathrm{M}}} \cdot \boldsymbol{S}_2 \end{bmatrix} \cdot \boldsymbol{v}_{\mathrm{M}} \tag{5}$$

The warping can then be obtained from transverse displacement u by the inverse matrix of S_1:

$$\boldsymbol{v}_{\mathrm{M}} = \boldsymbol{S}_3 \cdot \boldsymbol{u} \tag{6}$$

With the small modification of axial mode, Eq. (6) demonstrates the feasibility of using transverse displacement to obtain longitudinal displacement (warping). This could be applied to establish the mode classes GDL.

2.2 GDL transverse displacements

International system of units (SI) are required, and other unit systems are optional. The suggested format is metric (US imperial optional) such as 2.3 mm (0.091 inch). This includes units in the main body of the paper, tables, and figures.

1) G modes satisfy the rigid-body deformation:

$$\boldsymbol{u}^{\mathrm{G}} = \boldsymbol{R}_{\mathrm{u}}^{\mathrm{G}} \cdot \boldsymbol{d}^{\mathrm{G}} \tag{7}$$

where $\boldsymbol{d}^{\mathrm{G}}$ is an arbitrary 3×1 vector and

$$\boldsymbol{R}_{\mathrm{u}}^{\mathrm{G}} = \begin{bmatrix} \cos\boldsymbol{\alpha} & \sin\boldsymbol{\alpha} & \boldsymbol{r} \end{bmatrix} \tag{8}$$

where, $\boldsymbol{\alpha}$ is a column vector of the inclined angle from middle-line plates (i.e., local x- axis) to the global X- axis, and $\boldsymbol{r}$ is a column vector of the distances from the origin to transverse tangential displacements.

2) For D modes, the class cFSM utilizes the orthogonality of the warping displacements with G:

$$\int_A v^{\mathrm{G}} \cdot v^{\mathrm{D}} \cdot \mathrm{d}A = 0 \tag{9}$$

which can be written,

$$\left\{\boldsymbol{v}_{\mathrm{M}}^{\mathrm{G}}\right\}^{\mathrm{T}} \cdot \boldsymbol{S}_2 \cdot \boldsymbol{v}_{\mathrm{M}}^{\mathrm{D}} = 0 \tag{10}$$

Substitute Eqs. (6) and (7) into Eq. (10), transverse displacement $\boldsymbol{u}^{\mathrm{D}}$ of D modes can be rewritten from Eq. (10),

$$\boldsymbol{u}^{\mathrm{D}} = \boldsymbol{R}_{\mathrm{u}}^{\mathrm{D}} \cdot \boldsymbol{d}^{\mathrm{D}} \tag{11}$$

where $\boldsymbol{d}^{\mathrm{D}}$ is an arbitrary (n_{M}-4)×1 vector.

3) For L modes, it satisfies $\boldsymbol{v}_{\mathrm{M}} = \boldsymbol{0}$, which can be written as

$$\boldsymbol{v}_{\mathrm{M}}^{\mathrm{L}} = 0 \tag{12}$$

From Eqs. (12) and (6), this means

$$\boldsymbol{u}^{\mathrm{L}} = 0 \tag{13}$$

Eq. (13) and Eq. (12) actually demonstrates the equivalence of the classic cFSM mode definitions and the current approach using transverse displacement $\boldsymbol{u}$.

2.3 GDL constraint matrices

For L modes, there a need for additional nodes in between main nodes – sub-nodes. For GD modes, longitudinal displaces of sub-nodes $\boldsymbol{v}_{\mathrm{S}}$ can be determined from $\boldsymbol{v}_{\mathrm{M}}$. The other transverse displacements and rotations of all nodes can be determined from the transverse displacement $\boldsymbol{u}$ [10]. Hence, all the nodal displacements can be obtained from $\boldsymbol{u}$

$$\boldsymbol{\Delta}^{\mathrm{GD}} = \boldsymbol{R}_{\Delta}^{\mathrm{GD}} \cdot \boldsymbol{u}^{\mathrm{GD}} \tag{14}$$

For D modes,

$$\boldsymbol{\Delta}^{\mathrm{D}} = \boldsymbol{R}^{\mathrm{D}} \cdot \boldsymbol{d}^{\mathrm{D}} \text{ and} \tag{15}$$

$$\boldsymbol{R}^{\mathrm{D}} = \boldsymbol{R}_{\Delta}^{\mathrm{GD}} \cdot \boldsymbol{R}_{\mathrm{u}}^{\mathrm{D}} \tag{16}$$

For G modes, with the axial mode as well

$$\boldsymbol{\Delta}^{\mathrm{G}} = \boldsymbol{R}^{\mathrm{G}} \cdot \boldsymbol{d}^{\mathrm{G}} \tag{17}$$

where, $\boldsymbol{d}^{\mathrm{G}}$ is an arbitrary 4×1 vector

$$\boldsymbol{R}^{\mathrm{G}} = \left[\, \boldsymbol{\Delta}^{\mathrm{G1}} \;\vdots\; \boldsymbol{R}_{\Delta}^{\mathrm{GD}} \cdot \boldsymbol{R}_{\mathrm{u}}^{\mathrm{G}} \,\right] \tag{18}$$

where, $\boldsymbol{\Delta}^{\mathrm{G1}}$ represents the axial mode, where all the warping DOFs are 1 and all others 0.

For L modes, they satisfy both Eqs. (12) and (13). Hence, as mentioned before, all other DOFs including the rotation, normal translation of sub-nodes and external main nodes can be determined the same as those in [9], [10]. Thus the constraint matrix can be written as:

$$\boldsymbol{\Delta}^{\mathrm{L}} = \boldsymbol{R}^{\mathrm{L}} \cdot \boldsymbol{d}^{\mathrm{L}} \tag{19}$$

For the Shear and Transverse extension (ST, or O modes in general), the constraint matrices can be determined similar to those in [9], [10].

With all the constraint matrices, the modal decomposition and identification can be performed for thin-walled members.

3. Numerical Example I: versus the classic cFSM

Though the implementation approach changes here, the underlying mode definitions did not change, thus the same cFSM results should be expected for open thin-walled members. Consider a lipped channel with a height of 120mm, a flange width of 80mm, a lip length of 20mm and a thickness of 1mm. The material is assumed to be linear elastic with a Young's modulus *E* of 210GPa and a Poisson's ratio *v* of 0.3. For the member under axial loading with mesh shown in Fig. 2, the modal decomposition results of L, D, and G modes from classic cFSM and cFSM in this paper are shown in Fig. 3 along with the signature curve. The same results of GDL modes can be found.

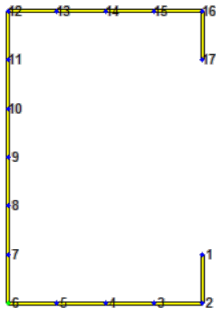

Fig. 2 A lipped channel with no rounded corner

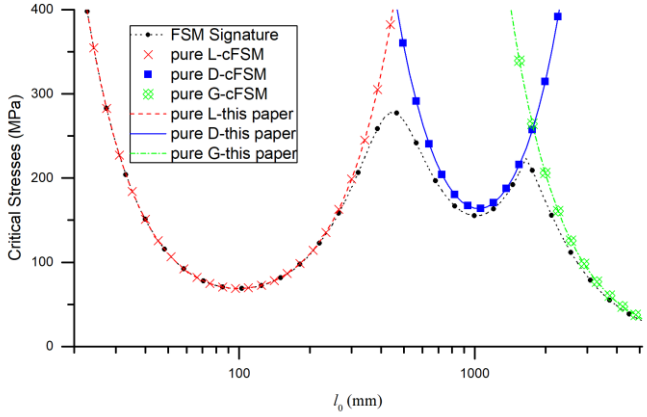

Fig. 3 Modal decomposition of a lipped channel under axial loading

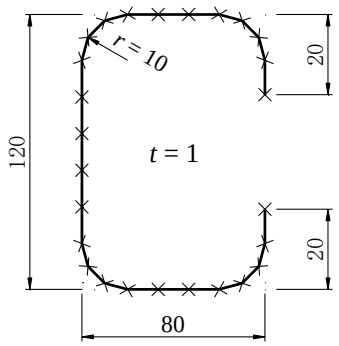

Fig. 4 A lipped channel with rounded corners

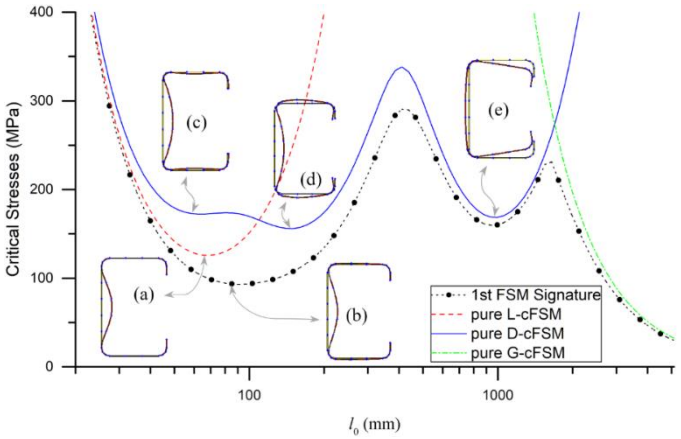

Fig. 5 Mode decomposition of a lipped channel with rounded corner under axial loading

4. Numerical Example II: rounded corner sections

For the same section in Section 3, rounded corners are considered in this section. The inner radius is 10mm. 3 intermediate nodes are used to approximate the corner as shown in Fig. 4. Under the axial load, the results of the FSM Signature curve is shown in Fig. 5. Either adopting the cFSM above defined or the classic cFSM in CUFSM (they are the same as illustrated in Section 3), the pure L, D, and G buckling curves are shown Fig. 5 along with several deformation modes. Clearly, for the L and D solutions, the cFSM show great discrepancies with the signature curves compared to the straight-line model in Section 3. From the deformation modes, it can be observed that the pure L buckling mode in Fig. 5(a)] shows no deformation at the round corner, with deformation concentrated in web. This is different from the L mode from signature curve in Fig. 5 (b) where rotation can be still observed around the corners even though the translation deformation is not obvious and this rotation forces the flange to have bending deformation as well. For this difference, the half-wave lengths of the pure L mode is smaller than that identified from the signature curve. In addition, the pure D mode solutions do not align with the straight-line model solutions and some of the modes predicted by the cFSM Fig. 5 (c) and (d) do not meet our engineering expectations at all.

This discrepancy is due to the corner nodes being treated as main nodes. For pure L modes, the bending interaction between flanges and web has been prevented due the corner main nodes; while for pure D modes, the warping at the corner main nodes can cause the ration of the corner region and correspondingly the bending of web and flange, which causes the deformation modes in Fig. 5 (c) and (d) - more like L modes being categorized as D modes.

4.1 Solution Method

To overcome this issue, the proposed solutions is to separate the displacement contribution of corner nodes from the D mode definition and insert this into the L mode definition. First, there is a need to understand the mechanism of D modes. Fig. 6 illustrates the transverse displacement ***u*** of the section in Fig. 1. Recall the equivalent multi-span beam model used in the class cFSM for GD modes in [8]. Excluding the axial mode and only consider the main nodes here, according to the equivalent multi-span beam model the external main node's normal force should be zero and moment at each main nodes should be zero. Thus independent DOFs of this equivalent multi-span beam are exactly the transverse displacements as shown in Fig. 6

of the section in Fig. 1. The stiffness equation of the equivalent multi-span beam can then be transformed into

$$\boldsymbol{N}_{\mathrm{u}} = \boldsymbol{K}_{\mathrm{u}} \cdot \boldsymbol{u} \tag{20}$$

In other words, the transverse displacement of GD modes can also be treated as the deformation due to the middle-line transverse force $\boldsymbol{N}_{\mathrm{u}}$ (including the rigid body deformation).

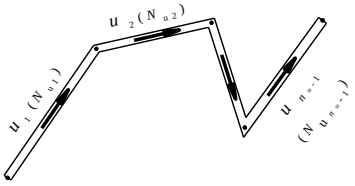

Fig. 6 Transverse displacements of GD modes

The transverse force $\boldsymbol{N}_{\mathrm{u}}$ of GD in the class cFSM is shown in **Error! Reference source not found.**(a) Fig. 4. To separate the displacement contribution of corner nodes from the D mode definition, the transverse force $\boldsymbol{N}_{\mathrm{u}}$ at the corner plates can be set as zero as shown in **Error! Reference source not found.**(b). The reduced D modes are designated as Dp modes here.

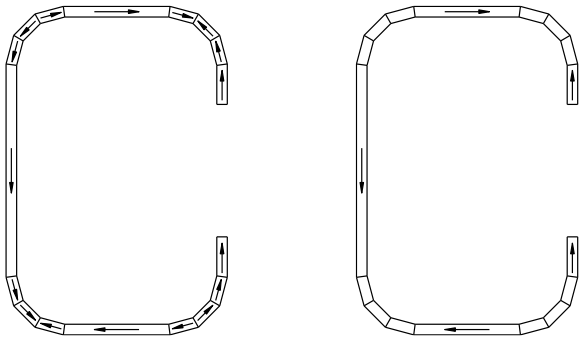

(a) in classic D mode (b) in reduced D mode - Dp

Fig. 7 Middle-line transverse force ($\mathbf{N}_{\mathrm{u}}$) in D modes

Designating the transverse displacement at the plates of the corners as $\boldsymbol{u}_{\mathrm{c}}$ and the rest as $\boldsymbol{u}_{\mathrm{p}}$, with $\boldsymbol{N}_{\mathrm{uc}} = \mathbf{0}$, $\boldsymbol{u}_{\mathrm{c}}$ can be determined by $\boldsymbol{u}_{\mathrm{p}}$ using the stiffness equation in Eq. (20). Hence the whole transverse displacement $\boldsymbol{u}$ can be determined by $\boldsymbol{u}_{\mathrm{p}}$,

$$\boldsymbol{u} = \boldsymbol{S}_{\mathrm{p}} \cdot \boldsymbol{u}_{\mathrm{p}} \tag{21}$$

Introduce this to Section 2 of the D modes, the constraint matrix of reduced Dp modes can be written as

$$\boldsymbol{\Delta}^{\mathrm{Dp}} = \boldsymbol{R}^{\mathrm{Dp}} \cdot \boldsymbol{d}^{\mathrm{Dp}} \tag{22}$$

Meanwhile, the part orthogonal with Dp in D modes can be designated as Dc modes to be inserted into L modes:

$$\boldsymbol{\Delta}^{\mathrm{Dc}} = \boldsymbol{R}^{\mathrm{Dc}} \cdot \boldsymbol{d}^{\mathrm{Dc}} \tag{23}$$

4.2 Application to rounded corner sections

The same section Fig. 4 is recalculated for the pure Dp (D modes for rounded corner sections) and L+Dc (L modes for rounded corner sections) modes in Fig. 8. The pure modes of D and L modes now agree well with the signature curves though slight differences do exist. If the 1st FSM Signature without ST (no Shear, no transverse extension) modes, the L+Dc shows excellent agreement with this FSM solutions.

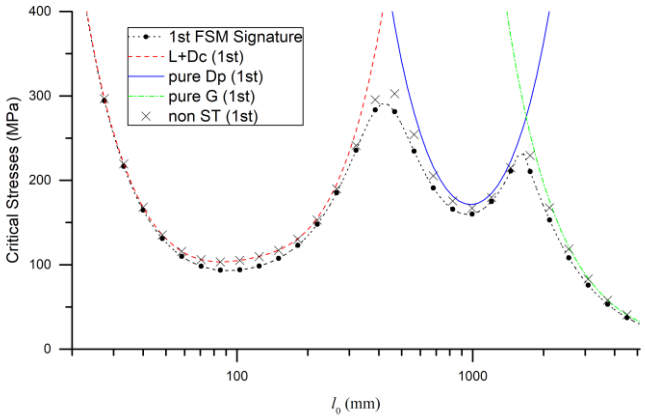

Fig. 8 Modal decomposition of rounded corner sections under axial loading

5. Numerical Example III: closed cross sections

The classic cFSM in CUFSM does not apply to closed sections as shown in Fig. 9. For the current cFSM, the exclusion of closed cross-sections is partially due to the superficial handling of in-plane shear deformations (i.e., shear modes).

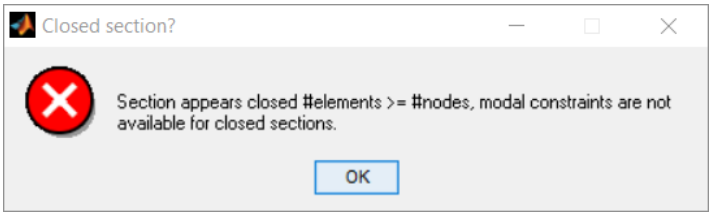

Fig. 9 Classic cFSM not able to handle closed cross sections

Consider a closed sections with q close loops, the main nodes is still n_{M}, however the total plate elements is no longer $(n_{\mathrm{M}} - 1)$, but $(n_{\mathrm{M}} - 1 + q)$. This renders the Eq. (5) no longer invertible. This is due to additional compatibility conditions due to close loops. Bredt shear strain can be introduced to bridge the additional compatibility between transverse and longitudinal displacements.

5.1 Introduce the Bredt shear strain

Assume a closed section with q closed loops and the j-th loop has i plate elements. If the *j-th* loop's Bredt shear force

is $f_j(y)$, then the Bredt shear stain of wall *i* corresponding to $f_j(y)$ is

$$\gamma_{i\_j}(y) = \frac{f_j(y)}{G \cdot t_i} \tag{24}$$

which leads to a transverse displacement of *i-th* plate as

$$\frac{\mathrm{d}}{\mathrm{d}y} u_{i\_j}(y) = \frac{f_j(y)}{G \cdot t_i} \tag{25}$$

Thus, with the Bredt shear forces for all loops, transverse displacements of the plates can be written as the following based on Eq.(25):

$$\frac{\mathrm{d}}{\mathrm{d}y} \boldsymbol{u}(y) = \frac{1}{G} \cdot \boldsymbol{S}_{\mathrm{B}} \cdot \boldsymbol{f}(y) \tag{26}$$

Integrate Eq. (26) from the end (i.e., where $y = 0$ and $\boldsymbol{u} = \boldsymbol{0}$) to the middle span (where $y = a/2$) and the transverse deformation at the middle-span section corresponding to Bredt shear strain:

$$\boldsymbol{u}_{\mathrm{B}} = \boldsymbol{S}_{\mathrm{B}} \cdot \boldsymbol{F} \tag{27}$$

where

$$\boldsymbol{F} = \frac{1}{G} \int_0^{\frac{a}{2}} \boldsymbol{f}(y) \mathrm{d}y \tag{28}$$

Combine Eqs. (27) and (2), the transverse displacement $\boldsymbol{u}$ can be written as

$$\boldsymbol{u} = \boldsymbol{S}_1 \cdot \boldsymbol{v}_{\mathrm{M}} + \boldsymbol{S}_{\mathrm{B}} \cdot \boldsymbol{F} \tag{29}$$

With the Eq. (4), now this can be rewritten as

$$\begin{Bmatrix} \boldsymbol{u} \\ 0 \end{Bmatrix} = \begin{bmatrix} \boldsymbol{S}_1 & \boldsymbol{S}_{\mathrm{B}} \\ \boldsymbol{1}_{1\times m} \cdot \boldsymbol{S}_2 & \boldsymbol{0}_{1\times q} \end{bmatrix} \cdot \begin{Bmatrix} \boldsymbol{v}_{\mathrm{M}} \\ \boldsymbol{F} \end{Bmatrix} \tag{30}$$

Here the matrix is a $(n_{\mathrm{M}} + q) \times (n_{\mathrm{M}} + q)$ invertible matrix, thus

$$\boldsymbol{v}_{\mathrm{M}} = \boldsymbol{S}_4 \cdot \boldsymbol{u} \tag{31}$$

Utilizing the transverse displacement $\boldsymbol{u}$, Eq. (30) demonstrates the possible inclusion of shear in closed loops in a concise format. Finally, for closed sections, the $\boldsymbol{S}_3$ matrix is needed to be replaced with $\boldsymbol{S}_4$ here for mode definitions.

5.2 Application to closed sections

The application of the modal decomposition of a closed section is shown in this section. The section is shown in Fig. 10 with a thickness of 1mm. The material is assumed to be linear elastic with a Young's modulus *E* of 210GPa and a Poisson's ratio *v* of 0. Three sub-nodes are used for each wall plate in FSM model. The modal decomposition results for this member under axial loading is shown in Fig. 11. Excellent agreement with signature curve can be observed.

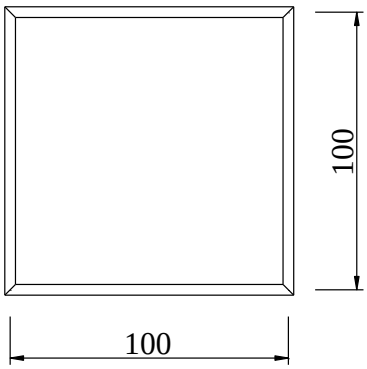

Fig. 10 A square steel tube

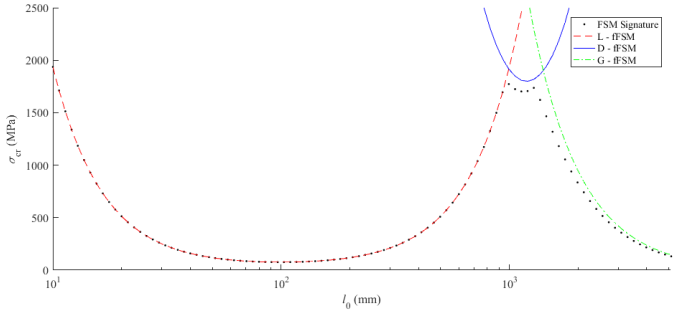

Fig. 11 Modal decomposition of the square steel tube under axial loading

6. Conclusions

This paper presents an enriched constrained Finite Strip Method (cFSM) to overcome the limits of the class cFSM in CUFSM. Current cFSM is limited to open sections and cannot handle rounded corners. The same mechanical criteria such as Vlasov's hypothesis, etc. are used here, however the implementation of these mode definition criteria is modified. The constraint matrices of Global (G), Distortional (D), and Local (L) modes are obtained through the transverse displacements instead of the longitudinal displacements (i.e., warping). The corner transverse displacements are separated from the classic D mode for sections with rounded corners and inserted into the L modes. The new cFSM solutions of pure L and D modes demonstrates excellent agreement with the signature curve and engineering expectations. Finally, the Bredt shear strain is introduced into the cFSM for closed sections and constraint matrices of mode classes are implemented based on the additional transverse displacements caused by Bredt shear. Modal decomposition of closed sections is then enabled.

7. Acknowledgments

The support of this work by the National Program on Key Research and Development Project (No. 2017YFC0703805) and the SUNY Poly SEED grant Track B (No. 917035-19) is gratefully acknowledged.

References

[1] L. G. Cheung, Y. K., and Tham, *The Finite Strip Method*. CRC, 1997.

[2] G. J. Hancock, "Local, Distortional and Lateral Buckling of I Beams," *J. Struct. Div. ASCE*, vol. 104, no. 11, pp. 1787–1798, 1978.

[3] AISI, "AISI S100-12: North American Specification for the Design of Cold-Formed Steel Structural Members." 2012.

[4] N. Silvestre and D. Camotim, "First-order generalised beam theory for arbitrary orthotropic materials," *Thin-Walled Struct.*, vol. 40, no. 9, pp. 755–789, 2002, doi: http://dx.doi.org/10.1016/S0263-8231(02)00025-3.

[5] N. Silvestre and D. Camotim, "Second-order generalised beam theory for arbitrary orthotropic materials," *Thin-Walled Struct.*, vol. 40, no. 9, pp. 791–820, 2002, doi: http://dx.doi.org/10.1016/S0263-8231(02)00026-5.

[6] C. Basaglia, D. Camotim, and N. Silvestre, "Non-linear GBT formulation for open-section thin-walled members with arbitrary support conditions," *Comput. Struct.*, vol. 89, no. 21–22, pp. 1906–1919, 2011, doi: 10.1016/j.compstruc.2011.07.001.

[7] R. Gonçalves and D. Camotim, "GBT deformation modes for curved thin-walled cross-sections based on a mid-line polygonal approximation," *Thin-Walled Struct.*, 2016, doi: 10.1016/j.tws.2015.12.025.

[8] S. Ádány and B. W. Schafer, "A full modal decomposition of thin-walled, single-branched open cross-section members via the constrained finite strip method," *J. Constr. Steel Res.*, 2008, doi: 10.1016/j.jcsr.2007.04.004.

[9] S. Ádány and B. W. Schafer, "Buckling mode decomposition of single-branched open cross-section members via finite strip method: Application and examples," *Thin-Walled Struct.*, 2006, doi: 10.1016/j.tws.2006.03.014.

[10] S. Ádány and B. W. Schafer, "Buckling mode decomposition of single-branched open cross-section members via finite strip method: Derivation," *Thin-Walled Struct.*, 2006, doi: 10.1016/j.tws.2006.03.013.

[11] Z. Li and B. Schafer, "Constrained Finite Strip Method for Thin-Walled Members with General End Boundary Conditions," *J. Eng. Mech.*, vol. 139, no. 11, pp. 1566–1576, 2013, doi: 10.1061/(ASCE)EM.1943-7889.0000591.

[12] S. Ádány, "Constrained shell Finite Element Method for thin-walled members, Part 1: constraints for a single band of finite elements," *Thin-Walled Struct.*, 2018, doi: 10.1016/j.tws.2017.01.015.

[13] S. Ádány, D. Visy, and R. Nagy, "Constrained shell Finite Element Method, Part 2: application to linear buckling analysis of thin-walled members," *Thin-Walled Struct.*, 2018, doi: 10.1016/j.tws.2017.01.022.

[14] S. Jin, Z. Li, F. Huang, D. Gan, R. Cheng, and G. Deng, "Constrained shell finite element method for elastic buckling analysis of thin-walled members," *Thin-Walled Struct.*, 2019, doi: 10.1016/j.tws.2019.106409.

[15] B. W. Schafer and S. Ádány, "Buckling analysis of cold-formed steel members using CUFSM: Conventional and constrained finite strip methods," in *Proceedings of the eighteenth international specialty conference on cold-formed steel structures*, 2006, pp. 39–54.

[16] Z. Li and B. W. Schafer, "Buckling analysis of cold-formed steel members with general boundary conditions using CUFSM: Conventional and constrained finite strip methods," in *20th International Specialty Conference on Cold-Formed Steel Structures - Recent Research and Developments in Cold-Formed Steel Design and Construction*, 2010.

[17] M. Khezri and K. J. R. Rasmussen, "An energy-based approach to buckling modal decomposition of thin-walled members with arbitrary cross-sections, Part 2: Modified global torsion modes, examples," *Thin-Walled Struct.*, 2019, doi: 10.1016/j.tws.2019.01.043.

[18] M. Khezri and K. J. R. Rasmussen, "An energy-based approach to buckling modal decomposition of thin-walled members with arbitrary cross sections, Part 1: Derivation," *Thin-Walled Struct.*, 2019, doi: 10.1016/j.tws.2019.01.041.

[19] M. Djelil, N. Djafour, M. Matallah, and M. Djafour, "Constrained spline Finite Strip Method for thin-walled members with open and closed cross-sections," *Thin-Walled Struct.*, 2018, doi: 10.1016/j.tws.2018.07.052.

[20] Z. Beregszászi and S. Ádány, "Modal buckling analysis of thin-walled members with rounded corners by using the constrained finite strip method with elastic corner elements," *Thin-Walled Struct.*, 2019, doi: 10.1016/j.tws.2019.04.058.

[21] J. Becque, "A new approach to modal decomposition of buckled shapes," *Structures*, 2015, doi: 10.1016/j.istruc.2015.10.011.

[22] S. Jin, D. Gan, H. Chen, R. Cheng, and X. Zhou, "A force-based method for identifying the deformation modes of thin-walled members," *Thin-Walled Struct.*, 2018, doi: 10.1016/j.tws.2018.04.008.

[23] Z. Li and B. W. Schafer, "The constrained finite strip method for general end boundary conditions," in *Structural Stability Research Council - Annual Stability Conference, SSRC 2010 - Proceedings*, 2010.